Constraining gluon shadowing using photoproduction in ultraperipheral pA and AA collisions

Adeola Adeluyi and C. A. Bertulani
Department of Physics & Astronomy, Texas A&M University-Commerce, Commerce, Texas 75428, USA
(Received 31 December 2011; revised manuscript received 23 February 2012; published 3 April 2012)

Photoproduction of heavy quarks and exclusive production of vector mesons in ultraperipheral proton-nucleus and nucleus-nucleus collisions depend significantly on nuclear gluon distributions. In the present study, we investigate quantitatively the extent of the applicability of these processes at the Large Hadron Collider in constraining the shadowing component of nuclear gluon modifications.

DOI: 10.1103/PhysRevC.85.044904 PACS number(s): 25.75.Cj, 24.85.+p, 25.40.Ve, 25.75.Dw

I. INTRODUCTION

Ultraperipheral relativistic heavy ion collisions can explore several aspects of particle and nuclear physics and have been extensively discussed in the literature (for a small sample, see, e.g., Refs. [1–13]). In a recent publication, we explored lead-lead peripheral collisions at energies available at the CERN Large Hadron Collider (LHC) to probe gluon distributions in nuclei [14]. Using recent gluon distributions from global fits to data, we investigated the sensitivity of direct photoproduction of heavy quarks and exclusive production of vector mesons to varying strength of gluon modifications. This idea, originally proposed in Ref. [7], can be used to constrain nuclear gluon distribution from data on production of heavy quarks and vector mesons.

In this article, we extend our previous work by considering both direct and resolved processes in the photoproduction of heavy quarks in ultraperipheral proton-lead (pPb) and lead-lead (PbPb) collisions at the LHC. We also consider, as an addition to the previous treatment, exclusive production of vector mesons in pPb collisions. Our main goal is to investigate quantitatively the extent of applicability of these processes in constraining nuclear gluon modifications. In order to present a self-contained report, we include all relevant results and discussions from our previous study.

The paper is organized as follows: below we briefly discuss the photon flux generated by one of the nuclei (or proton), making reference to several previous publications where it has been discussed in detail. Section II treats the photoprocesses considered in this study, as well as the input nuclear and photon parton distributions. In Sec. III we present the results of our calculations and a brief comment on theoretical errors. Our conclusion is contained in Sec. IV.

For a given impact parameter $\mathbf{b}$, the flux of virtual photons with photon energy k, $d^3N_\gamma(k,\mathbf{b})/dkd^2b$, is strongly dependent on the Lorentz factor γ. At the LHC at CERN, the Lorentz factor in the laboratory frame γ_L is 7455 for proton-proton (pp), 4690 for proton-lead (pPb), and 2930 for lead-lead (PbPb) collisions. The relationship between the Lorentz contraction factor associated with the relative velocity between the colliding nuclei and the collider energy per nucleon, E/A, in GeV, is given by $\gamma = 2\gamma_L^2 - 1 \approx 2(1.0735E/A)^2$. The photon flux also depends strongly on the adiabaticity parameter $\zeta = kb/\gamma$ [2–4]:

$$\frac{d^3N_\gamma(k,\mathbf{b})}{dkd^2b} = \frac{Z^2\alpha\zeta^2}{\pi^2kb^2}\left[K_1^2(\zeta) + \frac{1}{\gamma_L^2}K_0^2(\zeta)\right], \tag{1}$$

which drops off exponentially for $\zeta > 1$, above a cutoff energy determined essentially by the size of the nucleus, $E_{\rm cutoff} \sim \gamma \text{MeV}/b$ (fm).

For symmetric nucleus-nucleus (AA) collisions, such as PbPb collisions at the LHC, each nucleus can act equally as source or target of the photon flux. Integrating $d^3N_\gamma(k,\mathbf{b})/dkd^2b$ over impact parameters with the constraint of no hadronic interactions and accounting for the photon polarization yields the total photon flux $dN_\gamma^Z(k)/dk$ given by [5,11]

$$\frac{dN_\gamma^Z(k)}{dk} = 2\pi\int_{2R_A}^{\infty} db\, b\int_0^R \frac{dr\, r}{\pi R_A^2}\int_0^{2\pi} d\phi \times \frac{d^3N_\gamma(k, b + r\cos\phi)}{dkd^2b}, \tag{2}$$

with R_A the radius of the nucleus.

In the case of proton-nucleus (pA) collisions, the nucleus acts preferentially as the source and the proton as the target, leading predominantly to γp processes. But there is still a nonnegligible contribution from γA processes in which the proton acts as the source of photons and the nucleus as the target. Thus, expressions for both types of fluxes are required for pA collisions. The flux due to the nucleus (of charge Z) can be evaluated analytically and is given by [2],

$$\frac{dN_\gamma^Z(k)}{dk} = \frac{2Z^2\alpha}{\pi k}\left\{\zeta_R^{pA}K_0\left(\zeta_R^{pA}\right)K_1\left(\zeta_R^{pA}\right) - \frac{\left(\zeta_R^{pA}\right)^2}{2}\left[K_1^2\left(\zeta_R^{pA}\right) - K_0^2\left(\zeta_R^{pA}\right)\right]\right\}, \tag{3}$$

with reduced adiabaticity parameter, ζ_R^{pA}, given by $\zeta_R^{pA} = k(R_p + R_A)/\gamma$ and R_p the effective radius of the proton.

The flux due to the proton is usually estimated using the dipole formula for the electric form factor [15]:

$$\frac{dN_\gamma^p(k)}{dk} = \frac{\alpha}{2\pi k}\left[1 + \left(1 - \frac{2k}{\sqrt{S_{NN}}}\right)^2\right] \times \left(\ln D - \frac{11}{6} + \frac{3}{D} - \frac{3}{2D^2} + \frac{1}{3D^3}\right), \tag{4}$$

where $D = 1 + [0.71\,\text{GeV}^2/Q_{\rm min}^2]$ and the minimum momentum transferred $Q_{\rm min}^2 = k^2/[\gamma^2(1 - 2k/\sqrt{S_{NN}})]$.

With the knowledge of the photon flux, any generic total photoproduction cross section can be expressed as a convolution of a process cross section $\sigma_\gamma^X(k)$ and the photon

flux, dN_γ/dk. Thus, for AA collisions,

$$\sigma^X = 2\int dk\,\frac{dN_\gamma^Z(k)}{dk}\,\sigma^{\gamma A\to X}(k), \tag{5}$$

with dN_γ^Z/dk given by Eq. (2). The factor of 2 accounts for the source/target symmetry present in AA collisions. In the case of pA collisions, we have

$$\sigma^X = \int dk\left[\frac{dN_\gamma^Z}{dk}\,\sigma^{\gamma p\to X}(k) + \frac{dN_\gamma^p}{dk}\,\sigma^{\gamma A\to X}(k)\right], \tag{6}$$

with dN_γ^Z/dk and dN_γ^p/dk given by Eqs. (3) and (4), respectively. Relevant expressions for the rapidity distributions for both AA and pA collisions are given later.

II. PHOTON-HADRON INTERACTIONS IN ULTRAPERIPHERAL COLLISIONS

A. Photoproduction of heavy quarks

From the viewpoint of a Fock space decomposition, photon interactions with hadrons and nuclei can be classified as direct or resolved. In direct interactions, the photon behaves as a point-like particle ("bare photon"), while in resolved interactions the photon fluctuates into a quark-antiquark state or an even more complex partonic configuration consisting of quarks and gluons. The cross section for the photoproduction of a pair of heavy quarks, $\sigma^{\gamma H\to Q\overline{Q}X}(k)$, is thus a sum of both the direct and resolved contributions,

$$\sigma^{\gamma H\to Q\overline{Q}X}(k) = \sigma^{\gamma H\to Q\overline{Q}X}_{\rm direct}(k) + \sigma^{\gamma H\to Q\overline{Q}X}_{\rm resolved}(k). \tag{7}$$

Here H stands for a proton or a nucleus ($H \equiv p, A$) and the total photoproduction cross section is obtained by convoluting the equivalent photon flux, $dN_\gamma(k)/dk$, with $\sigma^{\gamma H\to Q\overline{Q}X}(k)$, as described by Eqs. (5) and (6) for AA and pA collisions, respectively.

Let us now consider both processes in some detail. At leading order (LO), photon-gluon fusion leading to the production of a heavy quark pair is the only subprocess relevant to direct photoproduction. In view of the high energies involved, perturbative QCD is applicable, and the direct photoproduction cross section can be expressed as a convolution of the partonic cross section for the subprocess $\gamma g \to Q\overline{Q}$ and the relevant nucleon or nuclear gluon distribution:

$$\sigma^{\gamma H\to Q\overline{Q}X}_{\rm direct}(s) = \int dx\,\sigma^{\gamma g\to Q\overline{Q}}(\hat{s})\,f_g^H(x,Q^2)\,\Theta(\zeta), \tag{8}$$

with x the momentum fraction carried by the gluon. We use m_Q for the mass of the heavy quark (charm or bottom), $s = W_{\gamma H}^2$ denotes the square of the center-of-mass energy of the photon-nucleus (or photon-nucleon) system, $\hat{s} = W_{\gamma g}^2$ that of the photon-gluon system, and $\zeta = \hat{s} - 4m_Q^2$. The gluon distribution in H, $f_g^H(x,Q^2)$, is evaluated at the pQCD factorization scale $Q^2 = W_{\gamma g}^2 = \hat{s}$. The function $\Theta(\zeta)$ enforces a minimum ("threshold") value of x, $x_{\rm min}$, on the integral given by $x_{\rm min} = 4m_q^2/W_{\gamma H}^2$.

The partonic photon-gluon fusion cross section is given by [16–18]

$$\sigma^{\gamma g\to Q\overline{Q}}(\hat{s}) = \frac{2\pi\,\alpha_{\rm em}\,\alpha_s(Q^2)\,e_Q^2}{\hat{s}}\left[\left(1+\beta-\frac{\beta^2}{2}\right)\times\ln\left[\frac{1+\nu}{1-\nu}\right]-(1+\beta)\nu\right], \tag{9}$$

with e_Q the electric charge of the heavy quark Q, α_{em} the electromagnetic coupling constant, $\beta = 4m_Q^2/\hat{s}$, and $\nu = \sqrt{1-\beta}$.

The resolved contribution is identical to the hadroproduction of heavy quarks, and at leading order, involves terms corresponding to gluon-gluon and quark-antiquark subprocesses. The resolved cross section can be written as

$$\sigma^{\gamma H\to Q\overline{Q}X}_{\rm resolved}(s) = \int d\tilde{x}\Big[f_g^\gamma(x_1,Q^2)f_g^H(x_2,Q^2)\sigma^{gg\to Q\overline{Q}}(\hat{s}) + \sum_q f_q^\gamma(x_1,Q^2)\big[f_q^H(x_2,Q^2) + f_{\bar{q}}^H(x_2,Q^2)\big]\sigma^{q\bar{q}\to Q\overline{Q}}(\hat{s})\Big]\Theta(\zeta), \tag{10}$$

where $d\tilde{x} \equiv dx_1dx_2$, $f_a^\gamma(x_1,Q^2)$ $[f_a^H(x_2,Q^2)]$ is the distribution of parton a with momentum fraction x_1 (x_2) in a photon (H), respectively, $\hat{s} = x_1x_2s$ and $\zeta = \hat{s} - 4m_Q^2$. The summation over q runs over the light flavors; i.e., $q = u, d, s$.

The partonic cross sections $\sigma^{gg\to Q\overline{Q}}(\hat{s})$ and $\sigma^{q\bar{q}\to Q\overline{Q}}(\hat{s})$ are given by [19–21]

$$\sigma^{gg\to Q\overline{Q}}(\hat{s}) = \frac{\pi\,\alpha_s^2(Q^2)}{3\hat{s}}\left[\left(1+\beta+\frac{\beta^2}{16}\right)\ln\left(\frac{1+\nu}{1-\nu}\right) - \left(\frac{7}{4}+\frac{31}{16}\beta\right)\nu\right] \tag{11}$$

and

$$\sigma^{q\bar{q}\to Q\overline{Q}}(\hat{s}) = \frac{8\pi\,\alpha_s^2(Q^2)}{27\hat{s}}\left[\left(1+\frac{\beta}{2}\right)\sqrt{1-\beta}\right]. \tag{12}$$

Here, β and ν are as defined previously.

It is often more enlightening to represent the cross section in terms of rapidity, that is, to consider rapidity distributions. The differential cross section with respect to the rapidity of the heavy quark pair, $d\sigma/dy$, is related to the differential cross section with respect to photon energy, $d\sigma/dk$, through the relation $d\sigma/dy = kd\sigma/dk$. The rapidity distribution can, therefore, be expressed as

$$\frac{d\sigma^{\gamma H\to Q\overline{Q}X}}{dy} = k\,\frac{dN_\gamma(k)}{dk}\,\sigma^{\gamma H\to Q\overline{Q}X}(k) \tag{13}$$

and scales directly with the photon flux dN_γ/dk. Thus, for pA collisions, with the convention that the proton is incident from the right and the nucleus from the left, the total rapidity distribution is

$$\frac{d\sigma^{pA\to Q\overline{Q}X}}{dy} = \left[k\,\frac{dN_\gamma^Z(k)}{dk}\,\sigma^{\gamma p\to Q\overline{Q}X}(k)\right]_{k=k_l} + \left[k\,\frac{dN_\gamma^p(k)}{dk}\,\sigma^{\gamma A\to Q\overline{Q}X}(k)\right]_{k=k_r}, \tag{14}$$

where k_l ($k_l \propto e^{-y}$) and k_r ($k_r \propto e^{y}$) simply denote photons from the nucleus and proton, respectively, and the fluxes dN_γ^Z/dk and dN_γ^p/dk are given by Eqs. (3) and (4). As remarked earlier, the fluxes have support only at small values of k, dying out exponentially at large k. Thus, the first term on the right-hand side (γp distribution) peaks at positive rapidities, while the second term (γA distribution) peaks at negative rapidities. Since both the fluxes and process cross sections are different, the total distribution is manifestly asymmetric, and the γp term dominates due to the much larger nuclear flux dN_γ^Z/dk.

The total rapidity distribution for AA collisions can likewise be written as

$$\frac{d\sigma^{AA\to Q\overline{Q}X}}{dy} = \left[k\,\frac{dN_\gamma^Z(k)}{dk}\,\sigma^{\gamma p\to Q\overline{Q}X}(k)\right]_{k=k_l} + \left[k\,\frac{dN_\gamma^Z(k)}{dk}\,\sigma^{\gamma A\to Q\overline{Q}X}(k)\right]_{k=k_r}, \qquad (15)$$

with k_l (k_r) simply denoting photons from the nucleus incident from the left (right) and the flux dN_γ^Z/dk given by Eq. (2). Here the process cross sections and the left/right fluxes are identical; thus, the respective rapidity distributions are mirror images of each other and, consequently, the total distribution is symmetric about midrapidity ($y = 0$).

B. Exclusive production of vector mesons

The cross section for the exclusive elastic photoproduction of a vector meson V on H ($H \equiv p, A$) can be written as

$$\sigma^{\gamma H\to VH}(k) = \left.\frac{d\sigma^{\gamma H\to VH}}{dt}\right|_{t=0}\int dt|F_H(t)|^2, \qquad (16)$$

where $d\sigma^{\gamma A\to VA}/dt|_{t=0}$ is the forward scattering amplitude and $F_H(t)$ is the form factor. The dynamical information is encoded in the forward scattering amplitude while the momentum transfer of the elastic scattering is determined by the form factor, which is, in general, dependent on the spatial attributes of the target H.

There have been studies of the photoproduction of J/Ψ and Υ in ultraperipheral collisions at LHC (see, for instance, Refs. [5,7,11,12,22–28]). In this work, we use the simple amplitude calculated from leading-order two-gluon exchange in perturbative QCD [29,30] and corrected for other relevant effects (such as relativistic corrections, inclusion of the real part of the scattering amplitude, next-to-leading order NLO effects, etc.; see, for instance, Refs. [31,32]) through a phenomenological multiplicative correction factor ζ_V.

For elastic photoproduction on protons, the corrected LO scattering amplitude can be written as

$$\left.\frac{d\sigma^{\gamma p\to Vp}}{dt}\right|_{t=0} = \zeta_V\,\frac{16\pi^3\alpha_s^2\,\Gamma_{ee}}{3\alpha M_V^5}[xg_p(x,Q^2)]^2. \qquad (17)$$

Here, M_V is the mass of the vector meson [J/Ψ and $\Upsilon(1s)$ in the present study], $x = M_V^2/W_{\gamma p}^2$ is the fraction of the nucleon momentum carried by the gluons, and $g_p(x, Q^2)$ is the gluon distribution in a proton, evaluated at a momentum transfer $Q^2 = (M_V/2)^2$. Γ_{ee} is the leptonic decay width and α_s (α) the strong (electromagnetic) coupling constant. Equation (17) is easily generalized to the nuclear case,

$$\left.\frac{d\sigma^{\gamma A\to VA}}{dt}\right|_{t=0} = \zeta_V\,\frac{16\pi^3\alpha_s^2\,\Gamma_{ee}}{3\alpha M_V^5}[xg_A(x,Q^2)]^2, \qquad (18)$$

where $g_A(x, Q^2) = g_p(x, Q^2) \times R_g^A(x, Q^2)$ is the nuclear gluon distribution and $R_g^A(x, Q^2)$ the gluon modification.

The correction factor ζ_V is estimated by constraining the calculated cross sections for elastic vector meson photoproduction on protons, $\sigma^{\gamma p\to Vp}(W_{\gamma p})$, to reasonably reproduce the photoproduction data from HERA: Ref. [33] for J/Ψ and Refs. [33–35] for $\Upsilon(1s)$. Further details can be found in Ref. [14]. In contrast to photoproduction of heavy quarks, the quadratic dependence of the cross section on the gluon distribution has the significant implication of making exclusive vector meson production a very sensitive probe of nuclear gluon modifications.

We now discuss the momentum-squared transferred dependence (t-dependence) of the cross section. For a proton, the standard practice is to parametrize the t-dependence in the form of a rapidly decreasing exponential function, $e^{b|t|}$, where b is referred to as the slope parameter. Integrating this function with respect to t gives a multiplicative factor $1/b$ with units GeV^2. In the case of a nucleus, the nuclear form factor $F_A(t)$ is given by the Fourier transform of the nuclear density distribution: $F_A(t) = \int d^3r\,\rho_A(r)\,e^{i\mathbf{q}\cdot\mathbf{r}}$, where q is the momentum transferred. For a heavy nucleus, it is customary to model the density distribution as a Woods-Saxon distribution with parameters from electron scattering, $\rho_A(r) = \rho_0/[1 + e^{[(r-R_A)/d]}]$, with central density ρ_0, radius R_A, and skin depth d. For ^{208}Pb in use at the LHC, $\rho_0 = 0.16/\text{fm}^3$, $R_A = 1.2A^{1/3}$ fm, and $d = 0.549$ fm [36].

For the proton, the photonucleon cross section $\sigma^{\gamma p\to Vp}(k)$ is obtained through

$$\sigma^{\gamma p\to Vp}(k) = \frac{1}{b}\left.\frac{d\sigma^{\gamma p\to Vp}}{dt}\right|_{t=0}, \qquad (19)$$

with slope parameter b. In the present study we employ $b = 4.5$ GeV^{-2}. The photonuclear cross section is given by

$$\sigma^{\gamma A\to VA}(k) = \left.\frac{d\sigma^{\gamma A\to VA}}{dt}\right|_{t=0}\int_{t_{\min}(k)}^{\infty} dt|F(t)|^2. \qquad (20)$$

Here, $t_{\min}(k) = (M_v^2/4k\gamma_L)^2$, as is appropriate for narrow resonances [27]. The total cross sections for pA and AA collisions are obtained by a convolution of $\sigma^{\gamma p\to Vp}(k)$ and $\sigma^{\gamma A\to VA}(k)$ with the relevant photon flux as described by Eqs. (6) and (5), respectively.

The photon energy, k, is related to the rapidity of the vector meson y by $k = (M_V/2)\exp(y)$. Thus, as in the case of photoproduction of heavy quarks, the differential cross section with respect to rapidity is given by $d\sigma^{\gamma H\to VH}/dy = (kdN_\gamma(k)/dk)\sigma^{\gamma H\to VH}(k)$, and the corresponding expressions for rapidity distributions in pA and AA collisions are of the forms given by Eqs. (14) and (15), respectively. The symmetry attributes of the distributions are also similar.

C. Parton distributions in nuclei and photons

We now turn to the consideration of the parton distributions (PDs) relevant to the processes considered in the present study. As mentioned earlier, the direct contribution to the photoproduction of heavy quarks is dependent solely on the gluon distributions in protons and nuclei, same as for the elastic photoproduction of vector mesons. The resolved contribution, on the other hand, requires the distributions of light quarks and antiquarks and gluons in photons, protons, and nuclei. Thus, in addition to the usual requirement of nucleon and nuclear parton distributions (nPDs), there is also the need for the relatively poorly known parton distributions in photons (γPDs), thereby increasing the level of the theoretical uncertainties in the calculation of photoproduction of heavy quarks. Although the direct contribution is dominant, this dominance does not vitiate the need to have a good control on the resolved contribution, especially for $b\bar{b}$ production, where the resolved components are quite sizable.

Let us first discuss nuclear parton distributions. It is rather well-known that the distributions of partons (i.e., quarks and gluons) in nuclei are quite different from the distributions in free nucleons; that is, they are "modified" by the complex, many-body effects in the nucleus. These nuclear effects are usually parametrized in terms of "nuclear modifications" $R_a^A(x, Q^2)$, which, in general, depend on the parton specie (a), the nucleus (A), momentum fraction x, and scale Q^2. The nuclear effects can be categorized based on different intervals in x. At small values of x ($x \lesssim 0.04$), we have the phenomenon generally referred to as shadowing. This is a depletion, in the sense that in this interval, the distribution of a parton a in the nucleus is smaller compared to the corresponding distribution in a free proton, i.e., $R_a^A < 1$. Antishadowing, which is an enhancement ($R_a^A > 1$), occurs in the range $0.04 \lesssim x \lesssim 0.3$. Another depletion, the classic EMC effect [37], is present in the interval $0.3 \lesssim x \lesssim 0.8$, while for $x > 0.8$, the Fermi motion region, we have another enhancement. It is important to note that although both shadowing and the EMC effect (antishadowing and Fermi motion) correspond to depletion (enhancement), the physical principles and mechanisms governing these phenomena are quite different. Further details can be found in Refs. [38–41]. With the knowledge of $R_a^A(x, Q^2)$, nuclear parton distributions can be expressed as a convolution of free nucleon parton distributions and nuclear modifications, i.e., $f_a^A(x, Q^2) = f_a(x, Q^2) \otimes R_a^A(x, Q^2)$.

While the determination of quark and antiquark distributions in nucleons and nuclei is, in general, a nontrivial task, that of gluons is even more problematic. Gluons are electrically neutral, and thus their distributions cannot be extracted directly from deeply inelastic scattering (DIS) and Drell-Yan (DY) processes, which account for the major part of the data used in global fits. Their distributions are, in general, inferred from sum rules and the Q^2 evolution of sea quarks distributions. The situation is even worse in the nuclear case: the available data is much less than for nucleons, and there is the added complication of a mass dependence. It is, therefore, not unusual for nuclear gluon distributions from different global fits to differ significantly, especially in the magnitude of the various nuclear effects

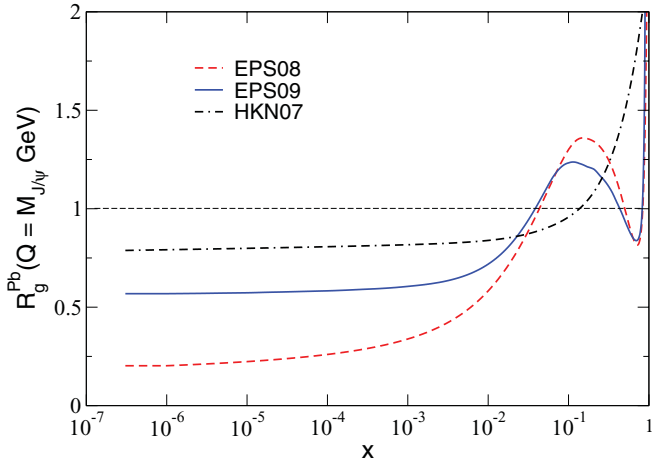

FIG. 1. (Color online) Nuclear gluon modifications in Pb, $R_g^{Pb}(x, Q^2 = M_{J/\Psi}^2)$, from EPS08 (dashed line), EPS09 (solid line), and HKN07 (dash-dotted line), respectively.

(shadowing, antishadowing, etc.). This is especially obvious at low Q^2 (i.e., around their initial starting scales) since evolution to high Q^2 tends to lessen the differences. Earlier global analyses [42–45] relied heavily on fixed-target nuclear DIS and DY lepton-pair production. Incorporation of data on inclusive hadron production in deuteron-gold collisions has been implemented in Refs. [46,47] and neutrino-iron data in Refs. [48–50]. We should also mention the approach in Refs. [51,52] utilizing the Gribov picture of shadowing. Despite all these advances, the nuclear gluon distribution is still currently the least constrained aspect of global fits to nuclear parton distributions, as significant uncertainties still persist at both small and large x.

Four recent nucleon and nuclear parton distributions are utilized in the present study. For the proton, we use the Martin-Stirling-Thorne-Watts (MSTW08) parton distributions [53], which are available up to next-to-next-to-leading order (NNLO). In the nuclear case, we use three nuclear modification sets. Two sets are by Eskola, Paukunnen, and Salgado, namely EPS08 and EPS09 [46,47]. The third is the Hirai-Kumano-Nagai (HKN07) distributions [45]. While EPS08 is only to leading order (LO), both EPS09 and HKN07 are available up to next-to-leading order (NLO). The distributions from MSTW08 serve two purposes: as the free nucleon distributions used in conjunction with nuclear modifications and also as a "special" nuclear distribution in the absence of nuclear effects. The latter case is particularly useful for highlighting the influence of the various nuclear effects on observables.

It is instructive to compare the characteristics of the gluon distributions from the four aforementioned sets based on the strength of their nuclear modifications. In Fig. 1 we show the nuclear modifications for gluons in Pb, $R_g^P b(x, Q^2)$ from EPS08, EPS09, and HKN07 at the factorization scale $Q^2 = M_{J/\Psi}^2$, appropriate for the elastic photoproduction of the J/Ψ meson. As already stated, one can view the MSTW08 gluon distribution as a nuclear gluon distribution in the limit of zero nuclear effects ($R_a^A = 1$). At this scale, HKN07 has a rather weak gluon shadowing, which extends well

into the antishadowing region, no antishadowing and gluon EMC effect, and an early onset of Fermi motion. EPS09 exhibits a moderately strong shadowing and appreciable antishadowing and EMC effect, with a quite strong Fermi motion. Nuclear modifications are strongest in EPS08: an especially strong shadowing and substantial antishadowing, EMC, and Fermi motion. Thus, in terms of shadowing we have a progression from zero effects to weak effects, moderate (intermediate) effects, then to strong effects as one progresses from MSTW08 to EPS08. The issue of uncertainties in parton distributions is becoming increasingly important, especially in relation to precision tests of QCD. Discussions on uncertainties in nuclear parton distributions can be found in Refs. [45–47].

Parton distributions in photons (γPDs) are derived from experimentally determined photon structure function $F_2^\gamma(x, Q^2)$, in conjunction with appreciable theoretical inputs. These inputs, which are necessary in implementing the parametrizations of photon parton distributions from the structure function, account in part for some of the observable differences in the available photon parton distribution sets. Another source of differences is in the choice and scope of experimental data from which F_2^γ is extracted. At present there is an appreciable number of photon parton distribution sets available, both at leading and next-to-leading orders [54–69]. It should be noted that unlike in the case of a nucleon, there are no valence quarks present in the photon; therefore, antiquark distributions are the same as quark distributions. Furthermore, there are no sum rules governing the gluon content; thus, the gluon distribution is almost totally unconstrained. The gluon distribution is a major contributor to $F_2^\gamma(x, Q^2)$ through the $\gamma^* g \to q\bar{q}$ channel, which has significant numerical support only at small x.

In light of the relatively poor situation, especially in the gluon sector, we use three different photon parton distribution sets in the present study. The rationale for this will become clear when we present results for the resolved component in heavy quark production. Two sets are relatively older and have been in common use: the Gluck-Reya-Vogt (GRV) set [60] and that by Schuler and Sjostrand (SaS1d) [64]. The third set, the Cornet-Jankowski-Krawczyck (CJK2) set [68], is more recent and has facility to estimate error on a calculated quantity due to the uncertainties in the input photon parton distributions. In Fig. 2 we show the parton distributions from these three sets for the light (u,d,s) quarks and gluon.

The up quark is the best constrained component of photon parton distributions, and even in this case there are clear differences between the three sets. This is also the case for the down quark. Only for the strange quark distribution is there good agreement between the three sets. But these differences pale in comparison with that of gluons, where the differences between the sets are quite significant almost across the whole x interval, with CJK2 having the largest magnitude, while SaS1d has the lowest, with the GRV somewhat intermediate. For the LO-resolved contribution to heavy quark photoproduction, the two competing partonic subprocesses are the $gg \to Q\bar{Q}$ and $q\bar{q} \to Q\bar{Q}$, and it is thus to be expected that significant differences will arise in the resolved cross sections whenever the $gg \to Q\bar{Q}$ component is appreciable.

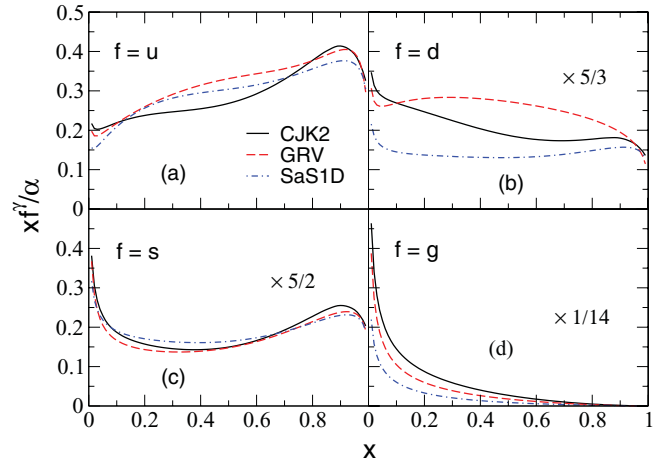

FIG. 2. (Color online) Parton distributions in the photon for (a) up, (b) down, (c) strange quarks, and (d) gluons at $Q^2 = 10\ \text{GeV}^2$ for three distribution sets: CJK2 (solid line) [68], GRV (dashed line) [60], and SaS1d (dash-dotted line) [64], respectively. For better visuality, the down quark distributions (b) have been enhanced by a factor of 5/3, the strange quark distributions (c) by 5/2, and the gluon distributions (d) by 1/14.

III. RESULTS

We now discuss the results of our calculations for both the inclusive photoproduction of heavy quarks ($c\bar{c}$ and $b\bar{b}$) and the exclusive elastic production of vector mesons [J/Ψ and $\Upsilon(1s)$] in pPb ($\sqrt{s_{NN}} = 8.8$ TeV) and PbPb ($\sqrt{s_{NN}} = 5.5$ TeV) collisions at the LHC. We take $m_c = 1.4$ GeV and $m_b = 4.75$ GeV for consistency with the MSTW08 parton distributions, and $m_{J/\Psi} = 3.097$ GeV and $m_\Upsilon = 9.46$ GeV, respectively. The strong coupling constant $\alpha_s(Q^2)$, needed for the calculations, is evaluated to one loop at the scale Q^2 using the evolution code contained in the MSTW08 package. Two comments pertaining to the results on photoproduction of heavy quarks are in order: first, due to the relative smallness of nuclear effects in heavy quark photoproduction, especially for pPb collisions, we have, for visual purposes, left out the results from the HKN07 distributions. In general, the HKN07 values are intermediate between those of EPS09 and MSTW08. Second, while we have used three sets of photon parton distributions in the calculations, we show only the rapidity distribution plots using the GRV set, since the GRV results are consistently somewhat intermediate between those from CJK2 and SaS1d distributions.

A. Heavy quarks in pA and AA collisions

1. Open charm

In Table I we present the cross sections for both direct and resolved $c\bar{c}$ production in ultraperipheral pPb collisions at the LHC, using the previously described nucleon/nuclear and photon parton distributions. Due to the large disparity in the magnitude of the photon fluxes from the proton and the nucleus (Pb), it is a common practice to neglect the photonuclear (γPb) contribution to the total cross section. Another simplification

TABLE I. Cross sections for photoproduction of $c\bar{c}$ in ultraperipheral pPb collisions at the LHC. All cross sections are in microbarns (μb).

	PDF	Direct	Resolved		
			SaS1d	GRV	CJK
γp	MSTW08	5570	692	1157	1418
	MSTW08	607	114	195	228
γA	EPS08	376	95	164	187
	EPS09	471	103	177	204

is the neglect of the resolved contribution which is relatively small in comparison with the dominant direct contribution. Since both the γPb and resolved contributions are dependent on nuclear and photon parton distributions, the results presented in Table I afford a good handle in determining the degree of validity of the above approximations for the rather significantly different attributes of the distributions utilized in the present study.

We first consider the photonuclear part. The γPb contribution to the total cross section is approximately 10.6% for MSTW08 (no nuclear modifications), 8.8% for EPS09 (moderate gluon shadowing), and 7.4% for EPS08 (strong gluon shadowing), almost totally independent of the choice of photon parton distribution set. The resolved contribution, on the other hand, while depending strongly on the choice of photon parton distributions, has an even more negligible dependence on the choice of nuclear parton distributions. For the SaS1d distribution, the resolved component is approximately 12%, while it is approximately 18% for the GRV distribution and 21% for the CJK2 set. As is to be expected, about 96% of the resolved component stems from γp, while about 90% of the γPb contribution derives from the direct component. Overall, the sensitivity to nuclear modifications (dominantly shadowing) is rather small: the no-modification (MSTW08) total cross section is reduced by approximately 4% and 2% by the modifications in EPS08 and EPS09, respectively. These features are manifestly exhibited in Fig. 3 where we display the direct and resolved components of both γp and γPb contributions to the rapidity distributions.

In Fig. 4 we show the rapidity distributions (sum of the components) with the GRV photon parton distributions. The left panel depicts the distributions separately for both γp and γPb contributions, while the right panel shows the total distributions, i.e., the sum of both contributions. As is apparent from the left panel, the γp contribution is dominant at all rapidities except for $y \lesssim -5$. In line with our convention, the γp contribution peaks at positive rapidities while the γPb distributions peak at negative rapidities, and the asymmetric nature of the total distributions is clearly exhibited. Despite the smallness of the γPb contribution, the effects of nuclear modifications are still slightly manifested in the total rapidity distributions shown in the right panel. It is interesting to note that the sensitivity to nuclear effects is significantly enhanced when one considers the ratio of the total rapidity distribution at a specific negative rapidity ($-y_1$), and the rapidity distribution at the equivalent positive rapidity ($+y_1$), somewhat reminiscent of pseudorapidity asymmetry in deuteron-gold collisions. The MSTW08 ratio for $y = -3, 3$ is reduced by about 9% and 5% by the modifications in EPS08 and EPS09, respectively, while for $y = -4, 4$ the reductions amount to 15% and 10%, and 23% and 14%, respectively, for $y = -5, 5$. Thus, the rapidity asymmetry ratio in the interval $-5 \leqslant y \leqslant 4, 4 \leqslant y \leqslant 5$ exhibits appreciable sensitivity to nuclear effects.

We now discuss the corresponding case of $c\bar{c}$ production in ultraperipheral PbPb collisions, and in Table II we show the cross sections (in mb) for both direct and resolved contributions.

The sensitivity to nuclear modifications (dominantly shadowing) is more significant here than in pPb collisions. Thus, considering the direct contribution, which is the dominant part, the modification-free (MSTW08) cross section is reduced by approximately 24% by the rather strong nuclear shadowing present in EPS08 and by about 14% in the case of EPS09. With the inclusion of the resolved component, the reductions are around 21% and 12%, respectively, and vary only slightly with the choice of photon parton distribution.

The resolved contribution exhibits a mild dependence on nuclear modifications and a much stronger sensitivity to photon parton distribution. Thus, in the case of SaS1d, the resolved component is 8.6% of the total cross section for

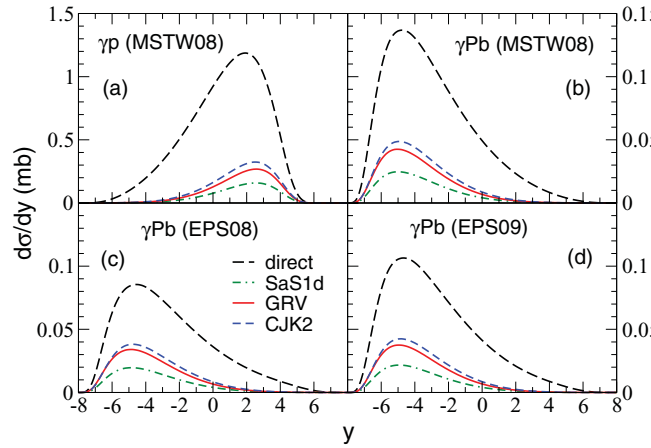

FIG. 3. (Color online) Direct (dashed lines) and resolved [solid (GRV), short-dashed (CJK2), dash-dotted (SaS1d) lines] components of γp and γPb contributions to rapidity distributions of $c\bar{c}$ photoproduction in pPb collisions at the LHC. (a) Depicts γp contribution with MSTW08 nucleon PDFs, while (b), (c), and (d) show γPb contributions using MSTW08 (no nuclear modifications), EPS08 (strong modifications), and EPS09 (moderate modifications) nuclear PDFs, respectively.

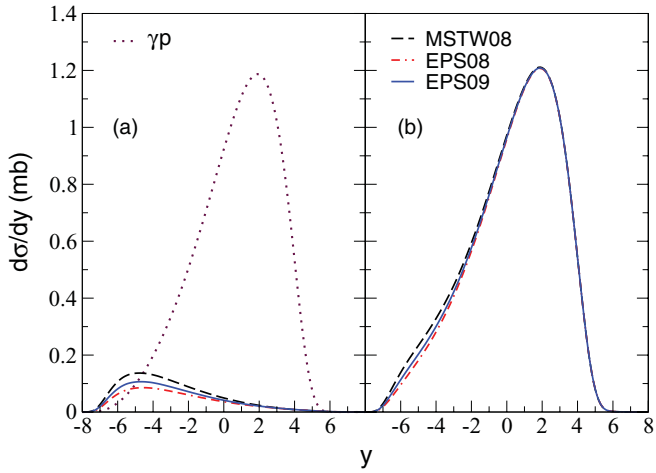

FIG. 4. (Color online) Rapidity distributions of $c\bar{c}$ photoproduction in pPb collisions at the LHC using the GRV photon parton distributions. In (a) we show the γp and γPb contributions to total rapidity distributions. Dotted line depicts the γp contribution, while the dashed (MSTW08), solid (EPS09), and dash-dotted (EPS08) lines correspond to γPb contributions with no shadowing, moderate shadowing, and strong shadowing, respectively. In (b) we present total rapidity distributions (sum of γp and γPb contributions).

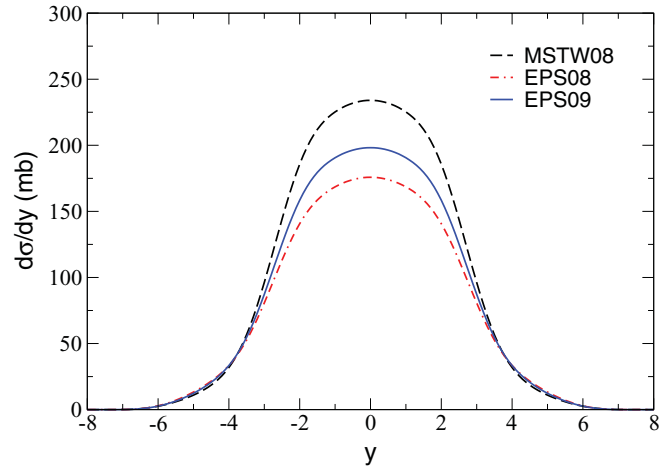

FIG. 5. (Color online) Total rapidity distributions of the photoproduction of $c\bar{c}$ in PbPb collisions at the LHC using the GRV photon parton distributions. Dashed line depicts result using the MSTW08 gluon distribution (no nuclear modifications). Solid and dash-dotted lines are results from nuclear-modified gluon distributions from EPS09 and EPS08, respectively.

MSTW08, 10.5% for EPS08, and 9.6% for EPS09. For GRV, the contributions are 13.4%, 16.2%, and 14.9%, respectively. The CJK2 values are the largest: 16.2%, 19.3%, and 17.9%, respectively.

The rapidity distributions for $c\bar{c}$ production in ultraperipheral PbPb collisions are shown in Fig. 5 and are manifestly symmetric about midrapidity ($y = 0$). The sensitivity to nuclear modifications is more transparent here than in total cross sections. Shadowing is the dominant nuclear effect for $-3 < y < 3$, and the rapidity distributions in this region reproduce the observed trend of gluon shadowing strength exhibited in Fig. 1. MSTW08 with its zero gluon shadowing gives the largest rapidity distribution while EPS08, with its strong gluon shadowing, gives the smallest. Due to strong flux suppression, shadowing is most markedly apparent for the rapidity range $-2 \lesssim y \lesssim 2$. This range therefore provides a good window to discriminate among different gluon shadowing scenarios.

The rapidity intervals $3 < y < 6$ corresponds to $x_{\rm min}$ in the antishadowing region (deep shadowing) for right (left) incident photons and vice versa for $-6 < y < -3$. Due to the photon flux suppression in the deep shadowing region, the rapidity distributions are sensitive mainly to antishadowing in addition to both EMC effect and Fermi motion. Since both EPS08 and EPS09 have substantial antishadowing, their rapidity distributions reflect this, being slightly larger than those from MSTW08. The discriminatory power here is not as appreciable as in the shadowing case, though, due largely to the smallness of the distributions.

For both rapidity ranges $y < -6$ and $y > 6$, $x_{\rm min} > 0.2$ and the relevant contributing nuclear effects are the EMC and Fermi motion since the contribution from antishadowing is small, and that from shadowing practically nonexistent by virtue of flux suppression. Both EPS08 and EPS09 nuclear modifications exhibit EMC effect and Fermi motion, and the destructive interference from both effects render their rapidity distributions to practically coincide with that from MSTW08.

TABLE II. Cross sections for photoproduction of $c\bar{c}$ in ultraperipheral PbPb collisions at the LHC. All cross sections are in millibarns (mb).

PDF	Direct	Resolved		
		SaS1d	GRV	CJK
MSTW08	1167	110	180	226
EPS08	890	104	172	213
EPS09	1002	106	176	219

2. *Open bottom*

We now discuss our results for total cross sections and rapidity distributions for $b\bar{b}$ production. In Table III we present the cross sections for both direct and resolved $b\bar{b}$ production in ultraperipheral pPb collisions at the LHC. In parallel with the treatment of $c\bar{c}$ production, we determine the relative importance of γPb and resolved contributions to the total $b\bar{b}$ production cross sections. For MSTW08 (no nuclear modifications), the γPb contribution to the total cross section is approximately 14%, 13% for EPS09(moderate gluon shadowing), and 12% for EPS08 (strong gluon shadowing), with little dependence on the choice of photon parton distribution set. It is thus apparent that while the photonuclear contribution is relatively more significant here than in $c\bar{c}$ production, the effect of nuclear shadowing is less. The resolved contribution again depends significantly on the choice of photon parton distribution and exhibits negligible dependence on the choice of nuclear parton distribution. For the SaS1d distribution, the resolved component is approximately 21%, while it is approximately 27% for the GRV distribution and 31% for

TABLE III. Cross sections for photoproduction of $b\bar{b}$ in ultraperipheral pPb collisions at the LHC. All cross sections are in nanobarns (nb).

	PDF	Direct	Resolved		
			SaS1d	GRV	CJK
γp	MSTW08	36512	8641	12178	14977
	MSTW08	5084	2061	3032	3663
γA	EPS08	3972	1936	2872	3451
	EPS09	4409	1988	2942	3543

the CJK2 set. These values are larger than the corresponding ones for $c\bar{c}$ production and thus serve to underscore the relatively higher importance of the resolved component in $b\bar{b}$ photoproduction. As noted above, the sensitivity to nuclear modifications (dominantly shadowing) is very small: the no-modification (MSTW08) total cross section is reduced by approximately 2.4% and 1.5% by the modifications in EPS08 and EPS09, respectively. Thus, with its appreciably large resolved component and weak sensitivity to nuclear effects, it is tempting to speculate that $b\bar{b}$ photoproduction could be of some use in constraining photon parton distributions.

In Fig. 6 we show the corresponding rapidity distributions for $b\bar{b}$ production using the GRV photon parton distributions. The left panel depicts the distributions separately for both γp and γPb contributions, while the right panel shows the total distributions, being the sum of both contributions. As is apparent from the left panel, the γp contribution is dominant at all rapidities except for $y \lesssim -4$. As in $c\bar{c}$ production, the γp contribution peaks at positive rapidities while the γPb distributions peak at negative rapidities, and the asymmetric nature of the total distributions is clearly manifested. Due to the smallness of the nuclear effects, the total rapidity distributions shown in the right panel almost overlap for the different

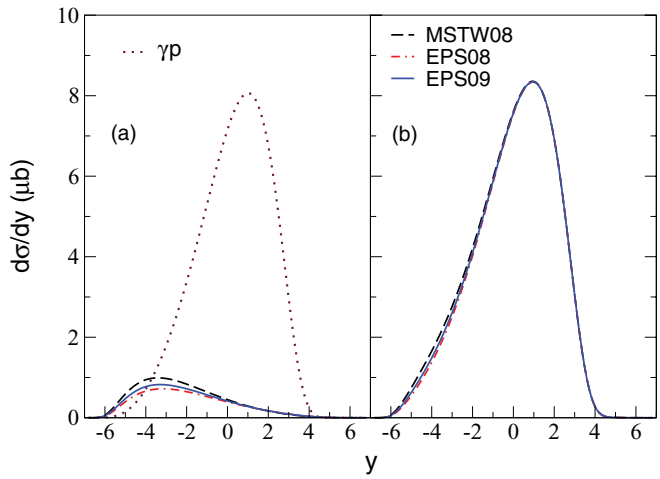

FIG. 6. (Color online) Rapidity distributions of $b\bar{b}$ photoproduction in pPb collisions at the LHC using the GRV photon parton distributions. In (a) we show the γp and γPb contributions to total rapidity distributions. Dotted line depicts the γp contribution, while the dashed (MSTW08), solid (EPS09), and dash-dotted (EPS09) lines correspond to γPb contributions with no shadowing, moderate shadowing, and strong shadowing, respectively. In (b) we present total rapidity distributions (sum of γp and γPb contributions).

nuclear parton distributions considered in the present study. Similar to $c\bar{c}$ production, the rapidity asymmetry ratio exhibits appreciable sensitivity to nuclear effects around $y = -4, 4$: the MSTW08 ratio is reduced by 19% and 6%, respectively, by the modifications in EPS08 and EPS09.

Let us now consider the corresponding case of $b\bar{b}$ production in ultraperipheral PbPb collisions. In Table IV we show the cross sections (in μb) for both direct and resolved contributions.

The sensitivity to nuclear modifications, while more appreciable here than in pPb collisions, is significantly less than for the equivalent $c\bar{c}$ production. The modification-free (MSTW08) cross section is reduced 5% by the modifications in EPS08 and about 3% in the case of EPS09. The resolved contribution is almost independent of nuclear modifications but exhibits a strong sensitivity to photon parton distribution. Thus, the resolved component is approximately 15% of the total cross section for SaS1d, 20% for GRV, and about 23% for CJK2. Again, these values indicate that the resolved component is relatively more significant in $b\bar{b}$ as compared to $c\bar{c}$ photoproduction.

In Fig. 7 we show the rapidity distribution for $b\bar{b}$ in ultraperipheral PbPb collisions at the LHC. Shadowing dominates in the rapidity interval $-2 < y < 2$ and is most clearly manifested in the rapidity window $-1 < y < 1$. Thus, this interval presents the best sensitivity to shadowing effects in $b\bar{b}$ production. Although less marked, the progression of rapidity distribution with relative shadowing strength follows the trend observed in $c\bar{c}$ production: MSTW08 still gives the largest distribution, while EPS08 gives the smallest. As in the case of $c\bar{c}$ production, there is a slight manifestation of the influence of antishadowing around $y = -3$ and $y = 3$. The distributions practically overlap for $y < -4$ and $y > 4$; thus, overall, the interval $-1 \lesssim y \lesssim 1$ seems to afford the best sensitivity to nuclear effects, in this case primarily shadowing. A detailed treatment of $b\bar{b}$ production at the LHC with emphasis on the x dependence can be found in Ref. [70].

TABLE IV. Cross sections for photoproduction of $b\bar{b}$ in ultraperipheral PbPb collisions at the LHC. All cross sections are in microbarns (μb).

PDF	Direct	Resolved		
		SaS1d	GRV	CJK
MSTW08	6227	1076	1468	1800
EPS08	5812	1097	1516	1867
EPS09	5992	1085	1496	1842

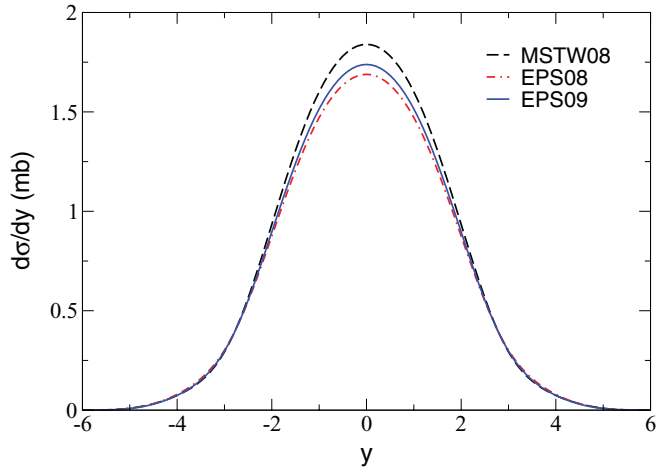

FIG. 7. (Color online) Total rapidity distributions of $b\bar{b}$ photoproduction in PbPb collisions at the LHC using the GRV photon parton distributions. Dashed line depicts result using the MSTW08 gluon distribution (no nuclear modifications). Solid and dash-dotted lines are results from nuclear-modified distributions from EPS09 and EPS08, respectively.

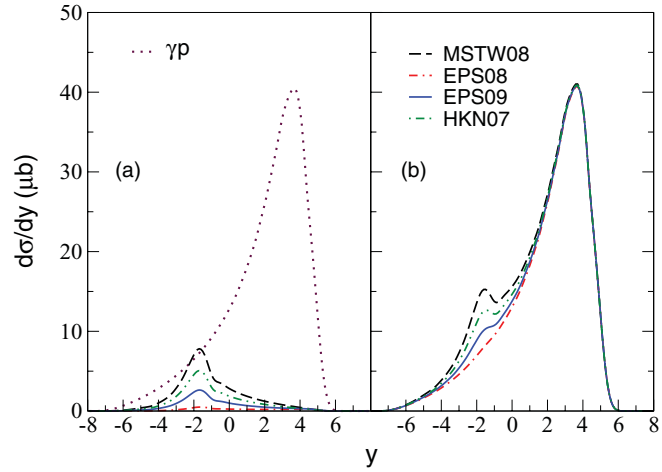

FIG. 8. (Color online) Rapidity distributions of exclusive photoproduction of J/Ψ in pPb collisions at the LHC. In (a) we show the γp and γPb contributions to total rapidity distributions. Dotted line depicts the γp contribution while the dashed (MSTW08), dash-double-dotted (HKN07), solid (EPS09), and dash-dotted (EPS08) lines correspond to γPb contributions with no shadowing, weak shadowing, moderate shadowing, and strong shadowing, respectively. In (b) we present total rapidity distributions (sum of γp and γPb contributions).

B. Vector mesons in pA and AA collisions

1. J/Ψ

We now present our results on elastic photoproduction of the J/Ψ and $\Upsilon(1s)$ in the framework of a corrected leading-order two-gluon exchange formalism in QCD. Here the nuclear effect (shadowing) is quite sizable; we therefore also display explicitly results from the HKN07 distribution set.

In Table V we present the components and total cross sections for the elastic photoproduction of J/Ψ in ultraperipheral pPb collisions at the LHC. As expected, the γp contribution is dominant, with the γPb contribution decreasing in size with increasing severity of gluon shadowing.

The contribution of the γPb component to the total cross section ranges from a high of about 12% for MSTW08 (no gluon shadowing) to a low of 1.3% for EPS08 (strong gluon shadowing), in accordance with the trend displayed in Fig. 1. This trend is replicated in the degree of shadowing reflected in the total cross section: the no-shadowing (MSTW08) cross section is reduced by about 11% by the shadowing in EPS08, 8% in EPS09, and 4% in HKN07, respectively.

Figure 8 shows the rapidity distributions for both γp and γPb components and their sums. The distributions are manifestly asymmetric, with the dominant γp component peaking at positive rapidities, while the subdominant γPb contributions peak at negative rapidities. The γPb distributions exhibit clearly the influence of gluon shadowing, especially in the narrow rapidity window $-3 \lesssim y \lesssim 1$, where the differences mimic the relative strength of gluon shadowing in the respective nuclear parton distribution. Although the γp contribution is dominant for practically all rapidities, these γPb distributions with the exception of EPS08 are appreciable enough in the said rapidity range such that the total rapidity distributions show the same tendency as that of the γPb component in the designated rapidity window. Thus, it seems feasible that a consideration of J/Ψ production in pPb collisions in this rapidity interval offers some potential in constraining gluon shadowing.

We now turn to J/Ψ production in ultraperipheral PbPb collisions at the LHC, and in Table VI we present the total cross sections from the different parton distributions. The differences in the predicted cross sections are extremely clear-cut, and thus this process can serve as an excellent probe of gluon shadowing as well as a good discriminator of the

TABLE V. Cross sections (in μb) for elastic photoproduction of J/Ψ in ultraperipheral pPb collisions at the LHC. Second and third columns are the contributions from γp and γPb, respectively, for different distributions. The sums of the two contributions are presented in the fourth column.

	γp	γA	Total
MSTW08	167.3	23.6	190.9
EPS08		2.2	169.5
EPS09		8.5	175.8
HKN07		15.4	182.7

TABLE VI. Total cross sections (in mb) for elastic photoproduction of J/Ψ in ultraperipheral PbPb collisions at the LHC.

PDF	Cross section
MSTW08	74
EPS08	10
EPS09	29
HKN07	49

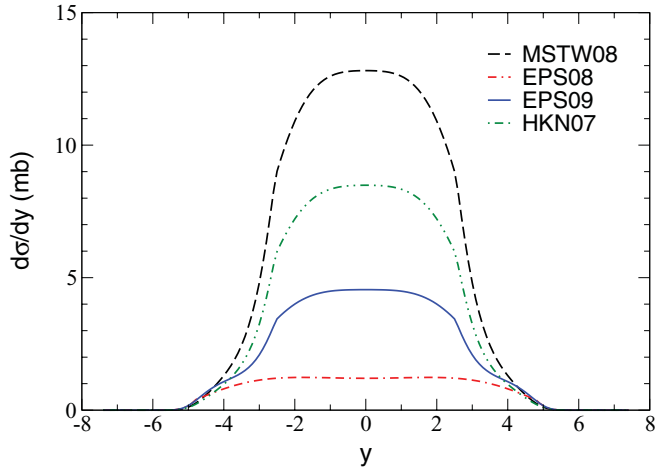

FIG. 9. (Color online) Total rapidity distributions of exclusive photoproduction of J/Ψ in PbPb collisions at the LHC. Dashed line depicts results using the MSTW08 gluon distribution (no nuclear modifications). Solid, dash-dotted, and dash-double-dotted lines are results from nuclear-modified gluon distributions from EPS09, EPS08, and HKN07 parton distributions, respectively.

different gluon shadowing templates considered in the current study.

It is instructive to consider the remarkable effect that the quadratic gluon dependence has on the cross sections (and also on the rapidity distributions). Thus, the no shadowing cross section is reduced by approximately 87% by the strong shadowing in EPS08 and by about 61% by the relatively moderate shadowing in EPS09. Even the rather weak gluon shadowing present in HKN07 is responsible for reducing the cross section by about 34%.

The constraining potential of the J/Ψ elastic production process is more clearly exhibited when rapidity distributions are considered. To this end we display the corresponding rapidity distributions in Fig. 9 for the four different gluon shadowing scenarios.

Shadowing is the relevant nuclear effect in the rapidity interval $-3 < y < 3$ and unsurprisingly, the rapidity distributions mimic the behavior in the shadowing region of Fig. 1. The largest rapidity distribution is given by MSTW08, followed by HKN07 and EPS09. The smallest is by EPS08 due to its strong gluon shadowing. The rapidity window $-2 < y < 2$ manifestly depicts the significant distinction between the various gluon distributions arising from the quadratic dependence. Antishadowing manifests in the intervals $-5 < y < -4$ and $4 < y < 5$; the effect, though, is quite slight.

2. $\Upsilon(1s)$

We now discuss our results for elastic production of $\Upsilon(1s)$ in ultraperipheral pPb and PbPb collisions. The ensuing treatment parallels closely that of J/Ψ in many respects due to the same underlying production mechanism.

In Table VII we present the components and total cross sections for the elastic photoproduction of Υ in ultraperipheral pPb collisions at the LHC. While the γp contribution is still dominant, the γPb contributions from the different gluon distributions are markedly significant and exhibit the trend of decreasing magnitude with increasing strength of gluon shadowing.

TABLE VII. Total cross sections (in nb) for elastic photoproduction of Υ in ultraperipheral pPb collisions at the LHC. Second and third columns are the contributions from γp and γPb, respectively, for different distributions. The sums of the two contributions are presented in the fourth column.

	γp	γA	Total
MSTW08	390	219	609
EPS08		84	474
EPS09		130	520
HKN07		161	551

The contribution of the γPb component to the total cross section is 36% for MSTW08 (no gluon shadowing), 29% for HKN07 (weak gluon shadowing), 25% for EPS09 (moderate gluon shadowing), and 18% for EPS08 (strong gluon shadowing). This gradation accords with the trend observed in Fig. 1, which is also replicated in the degree of shadowing reflected in the total cross section: the no-shadowing (MSTW08) cross section is reduced by about 22% by the shadowing in EPS08, 15% in EPS09, and 10% in HKN07, respectively. This appreciable magnitude of the effect of shadowing seems to indicate that Υ photoproduction cross section in ultraperipheral pPb collisions offers some promising potential in constraining nuclear gluon shadowing.

In Fig. 10 we show the rapidity distributions for both γp and γPb components (left panel) and the total (right panel). As usual, the distributions are asymmetric, with the

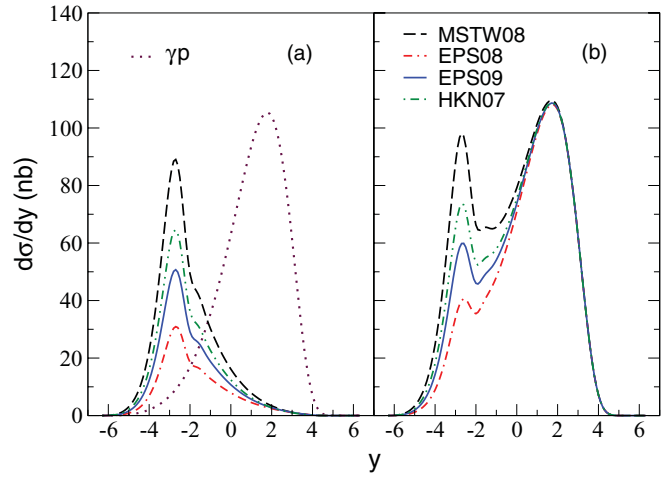

FIG. 10. (Color online) Rapidity distributions of exclusive photoproduction of $\Upsilon(1s)$ in pPb collisions at the LHC. In (a) we show the γp and γPb contributions to total rapidity distributions. Dotted line depicts the γp contribution while the dashed (MSTW08), dash-double-dotted (HKN07), solid (EPS09), and dash-dotted (EPS08) lines correspond to γPb contributions with no shadowing, weak shadowing, moderate shadowing, and strong shadowing, respectively. In (b) we present total rapidity distributions (sum of γp and γPb contributions).

TABLE VIII. Total cross sections (in μb) for elastic photoproduction of $\Upsilon(1s)$ in ultraperipheral PbPb collisions at the LHC.

PDF	Cross section
MSTW08	189
EPS08	99
EPS09	130
HKN07	146

dominant γp component peaking at positive rapidities while the subdominant γPb contributions peak at negative rapidities according to the convention adopted in the present study.

Let us consider the left panel. The γPb component distributions here, relative to that of γp, are more appreciable than for $J\Psi$ production. In fact, for $-5 \lesssim y \lesssim -2$, these distributions are larger than the γp distribution, and around their peaks at $y \sim -2.7$ they reflect quite distinctly the effect of the varying shadowing strength in the gluon distributions used. Thus, in the rapidity interval $-4 \lesssim y \lesssim -1$, the total distributions in the right panel show good sensitivity to gluon shadowing and, therefore, afford good potential for constraining purposes.

We now turn to Υ production in ultraperipheral PbPb collisions at the LHC. In Table VIII we present the total cross sections from the different gluon distributions.

Although not quite as dramatic as in the case of $J\Psi$ here also one can see the effect on the cross sections of the quadratic dependence on gluon distribution. The MSTW08 (no-shadowing) cross section is reduced by approximately 48% by the strong shadowing in EPS08, by about 31% by the relatively moderate shadowing in EPS09, and by 23% by the rather weak gluon shadowing present in HKN07. Thus, a consideration of the cross section can serve as a good probe of gluon shadowing as well as an efficient discriminator of the different gluon shadowing scenarios considered in the current study.

In order to further exhibit the constraining potentials of Υ photoproduction, we display the rapidity distributions in Fig. 11 for the four different gluon shadowing scenarios.

Shadowing remains the relevant nuclear modification for practically the entire rapidity range shown in the Fig. 11 and is markedly manifested in the interval $-2 < y < 2$. Thus rapidity distribution in this interval should be a good discriminator of gluon shadowing strength.

C. Theoretical errors and uncertainties in parton distributions

From a consideration of the general structure of the quantities (cross sections and rapidity distributions) considered in this study, three major sources of theoretical errors can be readily identified:

(i) accuracy of the relevant expressions for the photon flux,
(ii) higher-order corrections (neglect of terms greater than leading order in the case of photoproduction of heavy quarks, the accuracy of mopping up higher-order corrections with data from HERA in the case of production of J/Ψ and Υ),
(iii) uncertainties in the parton distributions.

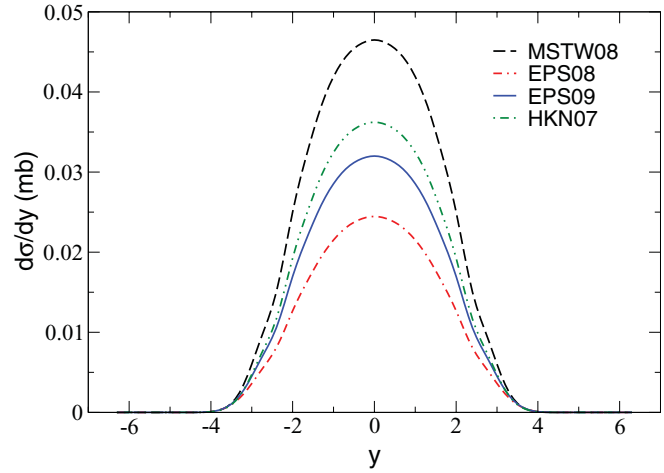

FIG. 11. (Color online) Total rapidity distributions of exclusive photoproduction of $\Upsilon(1s)$ in PbPb collisions at the LHC in the modified hard sphere density distribution approximation. Dashed line depicts result using the MSTW08 gluon distribution (no nuclear modifications). Solid, dash-dotted, and dash-double-dotted lines are results from nuclear-modified gluon distributions from EPS09, EPS08, and HKN07 parton distributions, respectively.

Here we give a brief qualitative comment on the third, i.e., the effects of uncertainties in parton distributions on our calculations. Let us first consider uncertainties in nPDs. This relevant for the dominant direct contribution in photoproduction of heavy quarks and elastic production of vector mesons. Both HKN07 [45] and EPS09 [47] have facilities for estimating error in the determination of a nPDs-dependent quantity like the cross section due to the uncertainties in the nuclear parton distributions. The HKN07 set achieves this through the availability of a set of gradient functions while EPS09 has thirty error sets to be used in conjunction with free proton parton distributions error sets.

For technical reasons we have not computed errors on cross sections using either of these two sets. Since this is a continuation of our earlier study, we have maintained the usage of the MSTW08 set for the free proton parton distributions while the EPS09 error evaluation is better handled with the CTEQ sets [71] of nucleon parton distributions. In the case of HKN07, we have used the nuclear modifications in our calculations, whereas the gradient terms are for the parton distributions proper. We thus advocate that the spread in the results involving the nuclear parton distributions be taken as loosely indicative of the effect of the uncertainties in the nuclear PDs.

We now consider the resolved component of photoproduction of heavy quarks where photon parton distributions are required. Among the available sets of photon parton distributions, only the CJK set has the facility to compute errors from uncertainties in photon PDs in terms of a tolerance parameter T [68,72], with the CJK2 uncertainty bands generated with $T = 5$. Thus, in principle, one needs only the CJK2 best fit and the associated error sets in order to compute the errors in the resolved contribution due to uncertainties in γPDs. The problem here is that the SaS1d distributions seems to lie consistently outside the CJK2 parton distributions error bands

(further details can be found in Ref. [72]). A reflection of this trend can be seen in our results for the resolved component, where the CJK2 values are consistently about a factor of two greater than the SaS1d values. As a test we have used the CJK2 error sets in conjunction with EPS09 to evaluate the uncertainty on the $c\bar{c}$ resolved cross section in PbPb collisions, with the result $\sigma^{\rm res}_{\rm CJK2} = 212.6 \pm 10.7\, T$ mb. The corresponding cross sections using SaS1d and GRV are $\sigma^{\rm res}_{\rm SaS1d} = 101.1$ mb and $\sigma^{\rm res}_{\rm GRV} = 169.3$ mb, respectively. Thus, the GRV result is already within the error limits of the CJK for $T \simeq 4$, whereas one needs $T \simeq 10.4$ in order to accommodate the SaS1d result. In view of this situation and since we have no cogent reason to exclude the SaS1d distributions, we have presented results from all three sets of γPDs and adopted the viewpoint espoused above that the spread in results should be taken rather loosely as an indicator of the effects of the uncertainties in the γPDs.

IV. CONCLUSIONS

In the present study, we have considered photoproduction of heavy quarks ($c\bar{c}$ and $b\bar{b}$) and elastic photoproduction of vector mesons [J/Ψ and $\Upsilon(1s)$] in ultraperipheral pPb and PbPb collisions at LHC. Both the dominant direct component in photoproduction of heavy quarks and elastic production of heavy mesons are dependent on nuclear gluon distributions and could, therefore, be potentially useful in constraining modifications such as shadowing and antishadowing in nuclear gluon distributions. The resolved component in photoproduction of heavy quarks depends on the distributions of light quarks and gluons in both photons and nuclei. Different sets of both nuclear and photon parton distributions with different attributes have been utilized.

In photoproduction of heavy quarks, the parton distribution dependence is linear and different modifications are superimposed due to the integration over the momentum fraction x. Despite these limitations, both cross sections and rapidity distributions for $c\bar{c}$ in PbPb collisions manifest appreciable sensitivity to shadowing around midrapidity and a slight sensitivity to antishadowing at more forward and backward rapidities. Thus, $c\bar{c}$ photoproduction offers good constraining potential for shadowing, and a somewhat less potential for antishadowing. Although photoproduction of $b\bar{b}$ is less sensitive to modifications than $c\bar{c}$, the influence of shadowing is evident around midrapidity, and it thus offers some constraining ability for shadowing. While both $c\bar{c}$ and $b\bar{b}$ total photoproduction cross sections and rapidity distributions in pPb collisions show little sensitivity to nuclear modifications, the rapidity asymmetry ratios in some select intervals do exhibit significant sensitivity. The resolved components are appreciable, especially for $b\bar{b}$, and are heavily dependent on the choice of γPDs. Thus, it seems feasible that they could be of some use in constraining photon parton distributions.

The outlook for constraining gluon shadowing is even better in the case of vector meson production. Here the quadratic dependence on gluon modifications makes elastic photoproduction of vector mesons particularly attractive for constraining purposes. The cross sections and rapidity distributions for both J/Ψ and $\Upsilon(1s)$ photoproduction in PbPb collisions exhibit very good sensitivity to gluon shadowing. Thus, both offer remarkable potential in constraining the shadowing component of nuclear gluon distributions. This is also true for Υ production and to a lesser extent $J\Psi$ production in pPb collisions.

ACKNOWLEDGMENTS

We acknowledge support by the US Department of Energy Grant No. DE-FG02-08ER41533 and the Research Corporation.

[1] E. Fermi, Z. Phys. **29**, 315 (1924); Nuovo Cimento **2**, 143 (1925).
[2] C. A. Bertulani and G. Baur, Phys. Rep. **163**, 299 (1988).
[3] R. N. Cahn and J. D. Jackson, Phys. Rev. D **42**, 3690 (1990).
[4] G. Baur and L. G. Ferreira Filho, Nucl. Phys. A **518**, 786 (1990).
[5] S. R. Klein and J. Nystrand, Phys. Rev. C **60**, 014903 (1999).
[6] C. A. Bertulani and D. S. Dolci, Nucl. Phys. A **674**, 527 (2000).
[7] V. P. Goncalves and C. A. Bertulani, Phys. Rev. C **65**, 054905 (2002).
[8] S. R. Klein, J. Nystrand, and R. Vogt, Phys. Rev. C **66**, 044906 (2002).
[9] V. P. Goncalves and M. V. T. Machado, Eur. Phys. J. C **31**, 371 (2003).
[10] C. A. Bertulani, S. R. Klein, and J. Nystrand, Annu. Rev. Nucl. Part. Sci. **55**, 271 (2005).
[11] A. J. Baltz *et al.*, Phys. Rep. **458**, 1 (2008).
[12] A. L. Ayala Filho, V. P. Goncalves, and M. T. Griep, Phys. Rev. C **78**, 044904 (2008).
[13] C. A. Salgado *et al.*, J. Phys. G **39**, 015010 (2012).
[14] A. Adeluyi and C. A. Bertulani, Phys. Rev. C **84**, 024916 (2011).
[15] M. Drees and D. Zeppenfeld, Phys. Rev. D **39**, 2536 (1989).
[16] M. Gluck and E. Reya, Phys. Lett. B **79**, 453 (1978).
[17] L. M. Jones and H. W. Wyld, Phys. Rev. D **17**, 759 (1978).
[18] H. Fritzsch and K. H. Streng, Phys. Lett. B **72**, 385 (1978).
[19] M. Gluck, J. F. Owens, and E. Reya, Phys. Rev. D **17**, 2324 (1978).
[20] B. L. Combridge, Nucl. Phys. B **151**, 429 (1979).
[21] R. Brock *et al.* (CTEQ Collaboration), Rev. Mod. Phys. **67**, 157 (1995).
[22] L. Frankfurt, M. Strikman, and M. Zhalov, Phys. Lett. B **540**, 220 (2002).
[23] V. P. Goncalves and M. V. T. Machado, Eur. Phys. J. C **40**, 519 (2005).
[24] V. P. Goncalves and M. V. T. Machado, Phys. Rev. D **77**, 014037 (2008).
[25] Yu. P. Ivanov, B. Z. Kopeliovich, and I. Schmidt, arXiv:0706.1532 [hep-ph].
[26] L. Frankfurt, V. Guzey, M. Strikman, and M. Zhalov, J. High Energy Phys. 08 (2003) 043.
[27] S. R. Klein and J. Nystrand, Phys. Rev. Lett. **92**, 142003 (2004).
[28] V. P. Goncalves and M. V. T. Machado, Phys. Rev. C **73**, 044902 (2006).
[29] M. G. Ryskin, Z. Phys. C **57**, 89 (1993).
[30] S. J. Brodsky, L. Frankfurt, J. F. Gunion, A. H. Mueller, and M. Strikman, Phys. Rev. D **50**, 3134 (1994).

[31] M. G. Ryskin, R. G. Roberts, A. D. Martin, and E. M. Levin, Z. Phys. C **76**, 231 (1997).
[32] L. Frankfurt, W. Koepf, and M. Strikman, Phys. Rev. D **57**, 512 (1998).
[33] C. Adloff *et al*. (H1 Collaboration), Phys. Lett. B **483**, 23 (2000).
[34] J. Breitweg *et al*. (ZEUS Collaboration), Phys. Lett. B **437**, 432 (1998).
[35] S. Chekanov *et al*. (ZEUS Collaboration), Phys. Lett. B **680**, 4 (2009).
[36] C. W. De Jager, H. De Vries, and C. De Vries, At. Data Nucl. Data Tables **14**, 479 (1974).
[37] J. J. Aubert *et al*. (European Muon Collaboration), Phys. Lett. B **123**, 275 (1983).
[38] D. F. Geesaman, K. Saito, and A. W. Thomas, Annu. Rev. Nucl. Part. Sci. **45**, 337 (1995).
[39] G. Piller and W. Weise, Phys. Rep. **330**, 1 (2000).
[40] N. Armesto, J. Phys. G **32**, R367 (2006).
[41] V. J. Kolhinen, arXiv:hep-ph/0506287.
[42] K. J. Eskola, V. J. Kolhinen, and C. A. Salgado, Eur. Phys. J. C **9**, 61 (1999).
[43] D. de Florian and R. Sassot, Phys. Rev. D **69**, 074028 (2004).
[44] M. Hirai, S. Kumano, and T. H. Nagai, Phys. Rev. C **70**, 044905 (2004); Nucl. Phys. Proc. Suppl. **139**, 21 (2005).
[45] M. Hirai, S. Kumano, and T. H. Nagai, Phys. Rev. C **76**, 065207 (2007).
[46] K. J. Eskola, H. Paukkunen, and C. A. Salgado, J. High Energy Phys. 07 (2008) 102.
[47] K. J. Eskola, H. Paukkunen, and C. A. Salgado, J. High Energy Phys. 04 (2009) 065.
[48] I. Schienbein, J. Y. Yu, K. Kovarik, C. Keppel, J. G. Morfin, F. I. Olness, and J. F. Owens, Phys. Rev. D **80**, 094004 (2009).
[49] T. Stavreva, I. Schienbein, F. Arleo, K. Kovarik, F. Olness, J. Y. Yu, and J. F. Owens, J. High Energy Phys. 01 (2011) 152.
[50] K. Kovarik, I. Schienbein, F. I. Olness, J. Y. Yu, C. Keppel, J. G. Morfin, J. F. Owens, and T. Stavreva, Phys. Rev. Lett. **106**, 122301 (2011).
[51] L. Frankfurt, V. Guzey, and M. Strikman, Phys. Rev. D **71**, 054001 (2005).
[52] L. Frankfurt, V. Guzey, and M. Strikman, Phys. Rept. **512**, 255 (2012).
[53] A. D. Martin, W. J. Stirling, R. S. Thorne, and G. Watt, Eur. Phys. J. C **63**, 189 (2009).
[54] D. W. Duke and J. F. Owens, Phys. Rev. D **26**, 1600 (1982).
[55] M. Drees and K. Grassie, Z. Phys. C **28**, 451 (1985).
[56] H. Abramowicz, K. Charchula, and A. Levy, Phys. Lett. B **269**, 458 (1991).
[57] K. Hagiwara, M. Tanaka, I. Watanabe, and T. Izubuchi, Phys. Rev. D **51**, 3197 (1995).
[58] M. Gluck, E. Reya, and A. Vogt, Phys. Rev. D **45**, 3986 (1992).
[59] M. Gluck, E. Reya, and M. Stratmann, Phys. Rev. D **51**, 3220 (1995).
[60] M. Gluck, E. Reya, and A. Vogt, Phys. Rev. D **46**, 1973 (1992).
[61] L. E. Gordon and J. K. Storrow, Nucl. Phys. B **489**, 405 (1997).
[62] L. E. Gordon and J. K. Storrow, Z. Phys. C **56**, 307 (1992).
[63] G. A. Schuler and T. Sjostrand, Phys. Lett. B **376**, 193 (1996).
[64] G. A. Schuler and T. Sjostrand, Z. Phys. C **68**, 607 (1995).
[65] P. Aurenche, J. P. Guillet, and M. Fontannaz, Z. Phys. C **64**, 621 (1994).
[66] P. Aurenche, P. Chiappetta, M. Fontannaz, J. P. Guillet, and E. Pilon, Z. Phys. C **56**, 589 (1992).
[67] F. Cornet, P. Jankowski, M. Krawczyk, and A. Lorca, Phys. Rev. D **68**, 014010 (2003).
[68] F. Cornet, P. Jankowski, and M. Krawczyk, Acta Phys. Pol. B **35**, 2215 (2004).
[69] F. Cornet, P. Jankowski, and M. Krawczyk, Phys. Rev. D **70**, 093004 (2004).
[70] M. Strikman, R. Vogt, and S. N. White, Phys. Rev. Lett. **96**, 082001 (2006).
[71] J. Pumplin, D. R. Stump, J. Huston, H. L. Lai, P. M. Nadolsky, and W. K. Tung, J. High Energy Phys. 07 (2002) 012.
[72] P. Jankowski, J. High Energy Phys. 05 (2004) 055.